Long-term stability studies of a semiconductor photoelectrode in three-electrode configuration†

Srinivas Vanka,[ab] Kai Sun,[c] Guosong Zeng,[d] Tuan Anh Pham,[e] Francesca Maria Toma,[d] Tadashi Ogitsu[e] and Zetian Mi *[a]

ABSTRACT: Improving the stability of semiconductor materials is one of the major challenges for sustainable and economic photoelectrochemical water splitting. N-terminated GaN nanostructures have emerged as a practical protective layer for conventional high efficiency but unstable Si and III–V photoelectrodes due to their near-perfect conduction band-alignment, which enables efficient extraction of photo-generated electrons, and N-terminated surfaces, which protects against chemical and photo-corrosion. Here, we demonstrate that Pt-decorated GaN nanostructures on an n^+–p Si photocathode can exhibit an ultrahigh stability of 3000 h (*i.e.*, over 500 days for usable sunlight ~5.5 h per day) at a large photocurrent density (>35 mA cm^{-2}) in three-electrode configuration under AM 1.5G one-sun illumination. The measured applied bias photon-to-current efficiency of 11.9%, with an excellent onset potential of ~0.56 V *vs.* RHE, is one of the highest values reported for a Si photocathode under AM 1.5G one-sun illumination. This study provides a paradigm shift for the design and development of semiconductor photoelectrodes for PEC water splitting: stability is no longer limited by the light absorber, but rather by co-catalyst particles.

Introduction

Photoelectrochemical (PEC) solar water splitting is one of the clean and sustainable approaches to convert the two most abundant natural resources on earth, *i.e.*, sunlight and water, into high calorific value, storable and clean chemical fuels such as hydrogen (H_2).[1–6] It is essential to develop high efficiency, durable, and cost-effective photoelectrode materials using industry-ready semiconductors for large-scale implementation of PEC devices.[5,7,8] To date, high efficiency photoelectrodes have been demonstrated using only a few semiconductors, including Si[6,9–13] and III–V compound semiconductors,[14–18] which, however, suffer from poor stability due to chemical and photochemical corrosion.[19–22] Compared to that of photovoltaic electrolyser (PV-EL) devices, the light absorber of PEC devices is often in direct contact with the electrolyte,[23] leading to more rapid degradation. The corrosion of semiconductors is influenced by many factors, including the intensity of light illumination, biasing conditions, catalyst, surface passivation, semiconductor electronic band structure, electrolyte composition, and interfaces of the semiconductor/electrolyte and catalyst/electrolyte.[6,19,20,24] These factors can be potentially addressed by exploring thermodynamic and kinetic protection schemes.

Gerischer's model[25] describes the thermodynamic considerations for photo-corrosion of a photoelectrode. To avoid competition between cathodic and anodic photo-corrosion of the photoelectrode with the hydrogen evolution reaction (HER) and oxygen evolution reaction (OER), respectively, it is vital that the photoelectrodes satisfy the basic criteria: $\phi^{h}_{corr} < E_{anodic}$ (1.23 V *vs.* RHE) and $\phi^{e}_{corr} > E_{cathodic}$ (0 V *vs.* RHE), where ϕ^{e}_{corr} is the energy level for the cathodic corrosion reaction of a semiconductor, and ϕ^{h}_{corr} is the energy level for the anodic corrosion reaction of a semiconductor. Previous studies[26,27] have shown that it is difficult to find an ideal semiconductor material that can satisfy both thermodynamic requirements simultaneously. Si can be easily oxidized under anodic conditions but is expected to be thermodynamically stable under cathodic conditions.[26] Other studies, however, suggested that Si could also get oxidized into an insulating oxide even under cathodic conditions,[24,28] which leads to poor stability. III–V compounds, such as GaAs, often undergo a chemical corrosion reaction due to accumulation of surface holes under dark and light conditions.[29] In this regard, various protection schemes have been

[a]*Department of Electrical Engineering and Computer Science, University of Michigan, Ann Arbor, 1301 Beal Avenue, Ann Arbor, MI 48109, USA. E-mail: ztmi@umich.edu; Tel: +1 734 764 3963*

[b]*Department of Electrical and Computer Engineering, McGill University, 3480 University Street, Montreal, Quebec, H3A 0E9, Canada*

[c]*Department of Materials Science and Engineering, University of Michigan, 2300 Hayward Street, Ann Arbor, MI 48109, USA*

[d]*Lawrence Berkeley National Laboratory, Chemical Sciences Division, 1 Cyclotron Road, Berkeley, CA 94720, USA*

[e]*Lawrence Livermore National Laboratory, Quantum Simulations Group, 7000 East Avenue, L-413, Livermore, CA 94550, USA*

† Electronic supplementary information (ESI) available. See DOI: 10.1039/c9ta09926c

developed to enhance the stability of photoelectrodes.[20] Kinetic protection for a given photoelectrode is possible by using a synergetic combination of a stable surface protective layer and a highly active co-catalyst.[19,20] The first generation of photoelectrodes often relies on coupling with highly active catalysts, as illustrated in Fig. 1(a), which can improve the stability due to the excellent reaction kinetics and more efficient charge carrier extraction. Recent studies have shown that hematite (α-Fe_2O_3) and bismuth vanadate ($BiVO_4$) with a NiFe co-catalyst exhibited a high level of stability with efficiencies reaching their theoretical maximum values.[30,31] Extensive studies have also been performed on the use of Pt,[32–35] MoS_2 [11,15,16,36,37] and NiMo[38,39] as both protective layers and co-catalysts for the HER. To further improve the device stability, the second generation of photoelectrodes, as illustrated in Fig. 1(b), employ relatively thick metal oxides, such as TiO_2,[27,40–42] Al_2O_3,[43] and IrO_x,[44] as

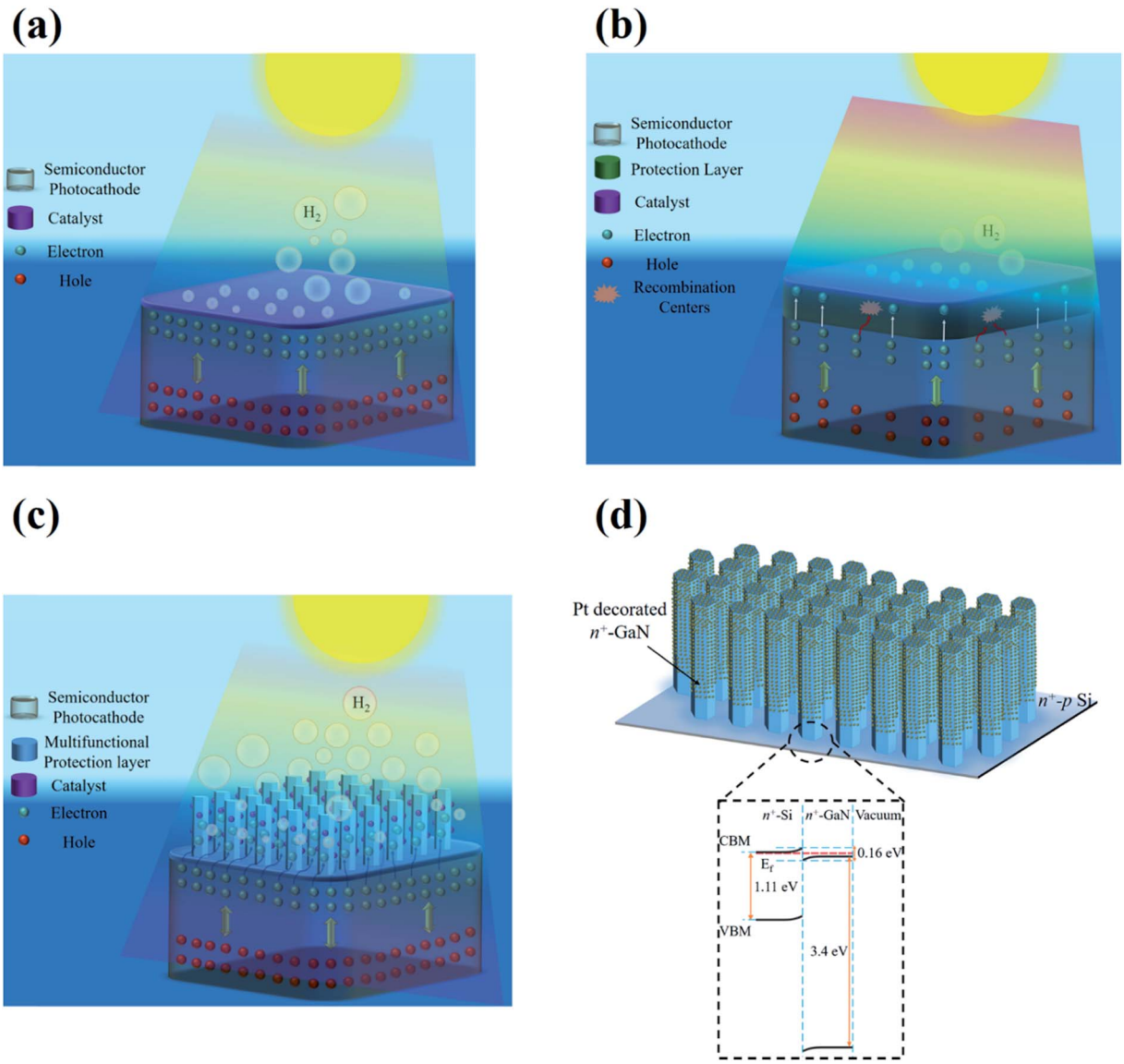

Fig. 1 Schematic illustration of the photoelectrochemical (PEC) photoelectrode and various surface protection schemes. (a) Illustration of a PEC device consisting of a semiconductor photoelectrode and a catalyst (pink color) on top. Photogenerated electrons (light cyan colored spheres) and holes (red colored spheres) are separated, and electrons are transferred to the catalyst active sites for proton reduction. (b) Illustration of the second generation of the surface protection scheme which consists of a semiconductor photoelectrode, a conventional thick protective layer (green color) and a catalyst. The device efficiency is often compromised with the use of such surface protection, due to parasitic light absorption, reduced charge carrier separation and extraction, and/or undesirable charge carrier recombination (recombination centers represented in a light orange color), which leads to lower H_2 production (grey bubbles). (c) Illustration of the third generation of the protection scheme, which consists of a semiconductor photoelectrode, a multi-functional protective layer (light blue color), and a catalyst. The protective layer is inherently stable in the electrolyte, which not only provides long-term stability but significantly enhances the light absorption, charge carrier separation, and extraction and further reduces surface recombination, thereby leading to enhanced efficiency. (d) Illustration of the Pt/n^+-GaN nanowires on the n^+–p Si photocathode as the third generation of the surface protection scheme. The band-diagram at the bottom shows the unique advantage of a negligible conduction band offset between n^+-GaN and n^+-Si, enabling efficient charge carrier extraction.[9]

passivation layers, in addition to the use of suitable co-catalysts.[27,44–46] Although the stability of these devices has improved, one major issue is the loss of photocurrent due to poor charge transfer and, in some cases, undesired light absorption by the protective layers.[19,21,47] One of the best-performing photocathodes, in terms of stability, was reported by Bae *et al.*[23] using a Pt co-catalyst and 100 nm thick TiO_2 for a metal oxide semiconductor junction Si photocathode, which exhibited stable operation for ~82 days with a photocurrent density ≤23 mA cm^{-2} (see Table S1, ESI†).

In this context, we envision that, to achieve both high efficiency and long-term stability, a multi-functional surface protection scheme should be developed, as schematically shown in Fig. 1(c). Such a protection scheme should offer not only robust surface protection but also significantly improved optical, electrical, and photoelectrochemical performance. In this study, we demonstrate such a unique class of photoelectrodes by integrating Pt-decorated N-rich GaN nanostructures with an n^+–p Si wafer. The N-terminated surfaces of GaN can protect the underlying Si absorber against photocorrosion and oxidation.[48–50] Unique to the GaN/Si heterointerface, the conduction band edges are near-perfectly aligned, thereby leading to efficient extraction of photo-generated charge carriers (electrons) from the underlying Si absorber, as schematically shown in Fig. 1(d). In this work we demonstrate that, with such a unique surface protection scheme, Si photocathodes can exhibit an ultrahigh stability of 3000 h with a stable photocurrent density between 37–38 mA cm^{-2} in 0.5 M H_2SO_4 under AM 1.5G one sun illumination in three-electrode configuration, which, to the best of our knowledge, is the longest stability ever measured for any photoelectrode material for H_2 production in a half-cell configuration (see Table S1, ESI†). The best performing platinized n^+-GaN nanowires/n^+–p Si photocathode showed an excellent onset potential (V_{on}) ~ 0.56 V *vs.* RHE with a high photocurrent density of ~37 mA cm^{-2} and a high applied bias photon-to-current efficiency (ABPE) of 11.9%. The device stability is further studied by using atomic force microscopy (AFM) measurements. Significantly, the utili-zation of GaN and Si, the two most produced semiconductor materials in the world, to realize high efficiency and highly stable photoelectrochemical water splitting provides a scalable and practical approach for solar fuel production.

Results and discussion

In this study, n^+-GaN nanowires were grown on an n^+–p Si wafer using a Veeco GEN II molecular beam epitaxy (MBE) system equipped with a radio frequency plasma-assisted nitrogen source (see the Experimental section, ESI†). The fabrication of the n^+–p Si substrate was discussed in previous reports.[9] As illustrated in Fig. 1(d), the conduction band minimum (CBM) for n^+-GaN is near-perfectly aligned with that for n^+-Si,[9] which was measured using XPS in previous studies.[9] Consequently, photo-generated electrons from the n^+–p Si substrate can be efficiently extracted by GaN nanowires, *i.e.*, with negligible resistivity, even when a relatively thick GaN protective layer is employed (see Fig. S2, ESI†), which is in direct contrast to the undesirable high resistivity associated with a relatively thick conventional protection scheme.[9,11,41,51] Fig. 2(a) shows the scanning electron microscope (SEM) image of the as-grown nanowires, which are vertically aligned with the Si substrate, with an average length ~ 400 nm and diameter ~ 40 nm. A detailed description of the photoelectrode preparation, including photo-deposition of Pt nanoparticles, is presented in the Experimental section, ESI.† The structural characterization after Pt photo-deposition for the samples was performed using scanning transmission electron microscopy (STEM). Fig. 2(b) shows the distribution of Pt nanoparticles around the GaN nanowires. In Fig. S1, ESI,† further STEM images are illustrated for the GaN nanowires after Pt deposition. Fig. 2(c) shows the linear scan voltammogram (LSV) of the Pt-decorated n^+-GaN nanowires on the n^+–p Si photocathode under AM 1.5G one sun illumination (red curve) and dark (black curve) conditions. The Pt/n^+-GaN nanowires/n^+–p Si photocathode showed excellent performance with an onset potential (V_{on}) of ~0.56 V *vs.* RHE and a high photocurrent density of ~37 mA cm^{-2} under AM 1.5G one-sun illumination in 0.5 M H_2SO_4. As shown in Fig. 2(d), the maximum ABPE (see the Experimental section, ESI†) for the Pt/n^+-GaN nanowires/n^+–p Si photocathode (red curve) is 11.9% at 0.38 V *vs.* RHE under AM 1.5G one sun illumination, which is one of the best reported values for Si photocathodes.[9,13,41,52] For the stability tests (both under dark and light conditions), we have chosen samples with an ABPE ≥ 10% and J at 0 V *vs.* RHE between 37–38 mA cm^{-2}.

Before starting the stability experiments, the electrode was thoroughly rinsed with distilled water and dried with a N_2 gun. The photoelectrode was then placed in 0.5 M H_2SO_4 inside a PEC chamber, and the stability experiment was conducted at a constant applied potential of 0 V *vs.* RHE under AM 1.5G one-sun illumination. Our initial studies, as described in previous reports, showed that a stability ~113 h can be achieved. Further stability testing, however, showed performance degradation (see Fig. S3(a), ESI†). In Fig. S3(b), ESI,† the STEM image shows a considerable loss of Pt nanoparticles on the GaN nanowire surface, which explains the poor onset potential. The photoelectrode material itself, including GaN and Si, showed no sign of degradation. To study the intrinsic stability of the GaN/Si photocathode, in this work we have employed a catalyst regeneration process, which was performed after approximately every 24 h of PEC experiments (see the Experimental section, ESI†). The entire process is schematically shown in Scheme S1, ESI.† After each catalyst regeneration, the J–V characteristics were measured under both dark conditions and AM 1.5G one-sun illumination and were compared to the 0^{th} h J–V characteristics (Fig. S4(a)–(c), ESI†). Then the experiment was resumed for the next cycle of the stability test and catalyst regeneration. The details of each regeneration cycle are summarized in Table S2, ESI.† It is important to mention here that after every 24 h of the experiment, the electrolyte was replaced with a fresh solution to maintain a constant pH ~ 0 for all the runs and to reduce possible carbonaceous contamination from epoxy.[23]

Fig. 3(a) shows the photocurrent density variation over the entire duration of 3000 h for the Pt/n^+-GaN nanowires/n^+–p Si photocathode under AM 1.5G one-sun illumination at 0 V *vs.*

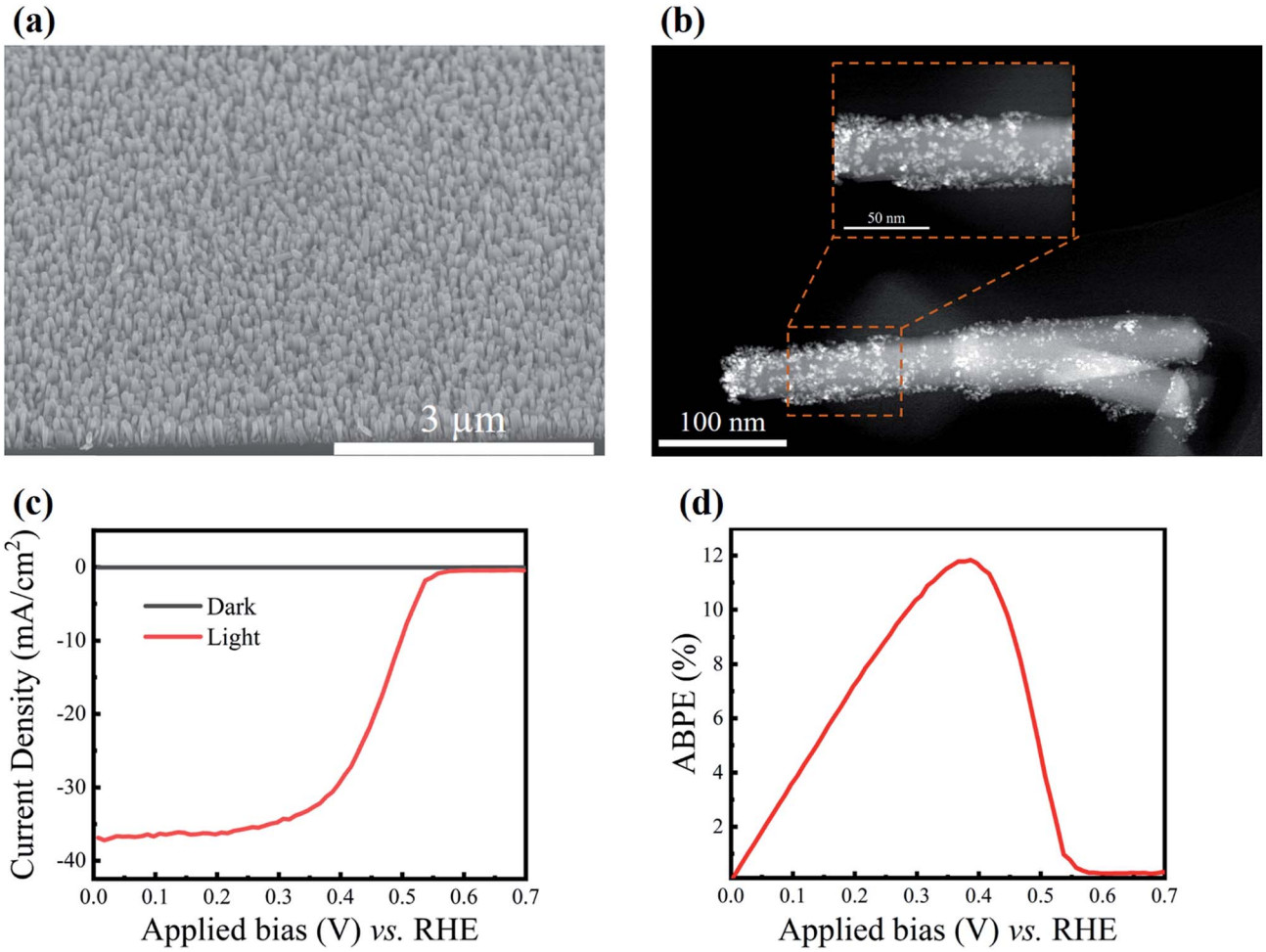

Fig. 2 Structural and PEC characterization of n^+-GaN nanowires on the n^+–p Si substrate. (a) 45° tilted SEM image of n^+-GaN nanowires on Si. (b) STEM image (HAADF) of a Pt nanoparticle decorated n^+-GaN nanowire. The inset is the magnified HAADF image of the highlighted box region (brown color) showing the distribution of Pt nanoparticles on the nanowire. (c) *J*–*V* curves of the platinized n^+-GaN nanowires/n^+–p Si photocathode under AM 1.5G one-sun illumination (red curve) and dark (black curve) conditions in 0.5 M H_2SO_4. (d) ABPE of the n^+-GaN nanowires/n^+–p Si photocathode under AM 1.5G one sun illumination.

RHE in 0.5 M H_2SO_4. As shown in Fig. 3(b), for 80–264 h of runs, *i.e.*, between the 4th and 12th regeneration cycles (see Table S2, ESI†), the photocurrent density varied between 36 and 40 mA cm^{-2}, which is within ±10% of the average J_0 value measured at 0 V *vs.* RHE. Fig. 3(c) shows that the variation of *J* increased to ~±20–25% from 1270 to 1539 h, *i.e.*, between the 59th and 73rd regeneration cycles (see Table S2, ESI†). These variations are mainly due to the unexpected epoxy meltdown, malfunctioning of the potentiostat (due to electrical fluctuations in the building) and poor back contact. In these cases, we had to stop the experiments and troubleshoot these issues, which led to an increase in the number of regeneration cycles as shown in Table S2, ESI.† The experimental problems were addressed during the subsequent runs by frequently redoing the back contact after every 100–120 h of runs and carefully monitoring the potentiostat during the cycles. Fig. 3(d) shows that the photocurrent variation for 2350–2640 h of runs (between the 113th and 125th regeneration cycles) is within ±10% of the J_0. It should be noted that despite photocurrent variations, the *J*–*V* characteristics at the start of the 141st regeneration cycle, *i.e.*, after 3008 h of runs with Pt redeposition, are nearly the same as the J_0 curve at the start of the experiments (see Fig. 3(e) and S4(d), ESI†), which implies that the GaN nanowires remain intact on the Si surface. Furthermore, Fig. 3(f) shows the variation of V_{on} for each regeneration cycle at the start (purple curve) and end (red curve) of each cycle. The slight reduction of V_{on} at the end of each regeneration cycle is due to the loss of some Pt nanoparticles as described earlier. The catalyst regeneration, at the start of each cycle, helps in immediately recovering the V_{on} for the LSV curves (see Fig. S4(d), ESI†).

Detailed structural characterization was further performed after 3000 h of experiments. The SEM image in Fig. 4(a) shows that there is virtually no change in the nanowire morphology compared to that of the as-grown samples. As illustrated in Fig. 4(b), the STEM image shows that the nanowire length is ~400 nm and the diameter is ~40 nm, which are nearly identical to those shown in Fig. 2(b). No apparent etching of the nanowire surface was observed. The inset in Fig. 4(b) shows the

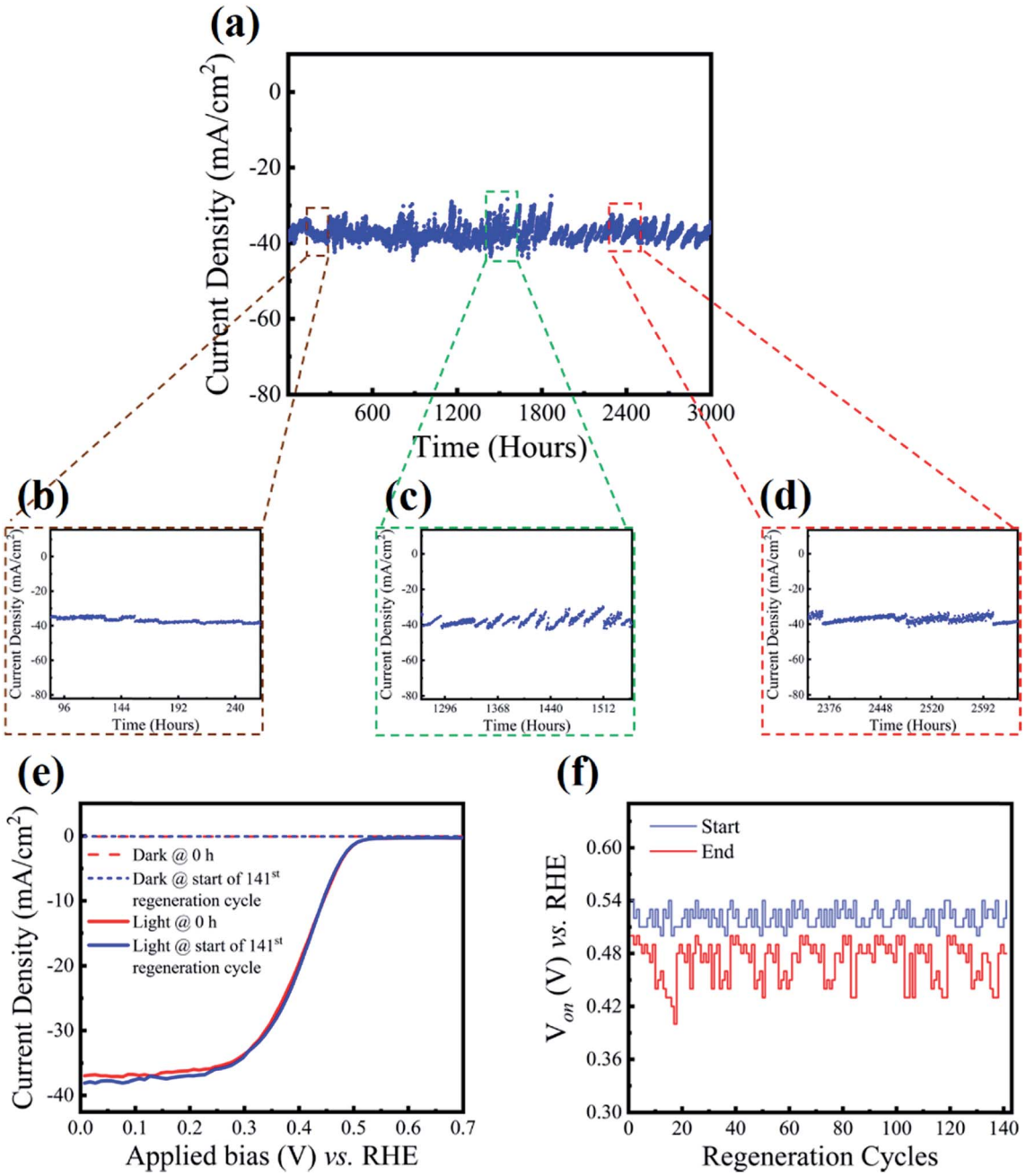

Fig. 3 Long term stability of the platinized n^+-GaN/n^+–p Si photocathode in three-electrode configuration. (a) Chronoamperometry long term stability measurements for the platinized n^+-GaN nanowires/n^+–p Si photocathode at 0 V *vs.* RHE in 0.5 M H_2SO_4 under AM 1.5G one sun illumination. (b) Stability results of the highlighted brown dashed box for 80–264 h of runs (4^{th} to 12^{th} regeneration cycles). (c) Stability results of the highlighted green dashed box for 1270–1539 h of runs (59^{th} to 73^{rd} regeneration cycles). (d) Stability results of the highlighted red dashed box for 2350–2640 h of runs (113^{th} to 125^{th} regeneration cycles). (e) LSV comparison between 0 h (red curves) and the start of the 141^{st} regeneration cycle (blue curves) under dark (dotted) and AM 1.5G one-sun illumination (solid) conditions in 0.5 M H_2SO_4. (f) V_{on} (*versus* RHE) variations at the start (purple) and end (red) of each regeneration cycle.

reduction of Pt nanoparticles on the nanowire compared to Fig. 2(b). More TEM images of the nanowires are shown in Fig. S5, ESI.† Due to the Pt nanoparticles falling off, the *J*–*V* curve immediately at the end of the 140^{th} regeneration cycle (see the blue curve in Fig. S4(c), ESI†) degraded somewhat. By performing Pt regeneration at the start of the 141^{st} regeneration cycle, the *J*–*V* characteristics were restored to the 0^{th} h curves (see Fig. S4(c), ESI†), which clearly shows that the GaN nanowires are still protecting the Si photocathode and the GaN-protected Si photocathode can last significantly longer than 3000 h. The dark currents before and after Pt regeneration for the 46^{th}, 96^{th}, and 140^{th} regeneration cycles (as shown in Fig. S4 and Table S2, ESI†) are nearly the same as the 0^{th} h dark current. In Fig. S6, ESI,† the ABPE for the 0^{th} h and at the start of the

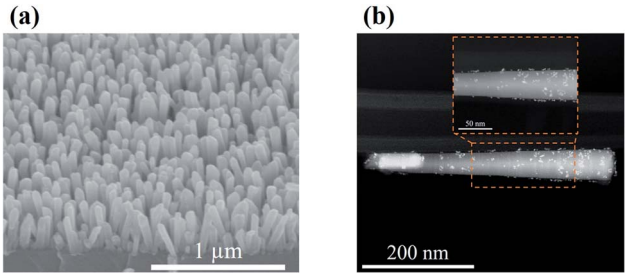

Fig. 4 Structural characterization of the platinized n^+-GaN/n^+–p Si photocathode after the stability test. (a) 45° tilted SEM and (b) STEM images of the Pt-decorated n^+-GaN nanowire/n^+–p Si photocathode after 3000 h of the stability experiment. The inset in (b): STEM HAADF image showing fewer Pt nanoparticles non-uniformly distributed on the highlighted (brown dashed box) segment of the n^+-GaN nanowire.

141st regeneration cycle under AM 1.5G one-sun illumination is found to be ~10%. These results are also consistent with the nearly identical X-ray diffraction measurements obtained for the sample before and after the stability test (see Fig. S7, ESI†). The dissolved Ga and Pt elements in the electrolyte are analyzed using inductively coupled plasma mass spectrometry (ICP-MS). The ICP-MS results for different runs (see Fig. S8 and the Experimental section, ESI†) show dissolved Ga concentrations of 15–20 nmol and Pt concentrations of 1–5 nmol, considering an error bar ~10% in the measurements. These results clearly show that GaN remains stable throughout the course of the stability test which agrees well with the above-mentioned STEM analysis.

We also evaluated the Faraday efficiency (see the Experimental section, ESI†) by analyzing H_2 generation from the Pt/n^+-GaN nanowires/n^+–p Si photocathode between 0 and 2 h and 3000 and 3002 h. As shown in Fig. 5(a), the photocurrent and H_2 evolution are simultaneously measured for the sample between 0 and 2 h at 0 V *vs.* RHE for a duration of 2 h in 0.5 M H_2SO_4 under AM 1.5G one sun illumination. Similarly, a H_2 evolution experiment was carried out for the sample between 3000 and 3002 h (shown in Fig. 5(b)) under the same conditions. In both cases, the Faraday efficiency is nearly 100%, considering that there is an error bar ~10% for H_2 sampling. Given the nearly identical LSV curves measured at 0 h and 3000 h, it is reasonably concluded that the GaN/Si photocathode can drive solar water splitting with a stability over 3000 h.

The total charge passed during the 3000 h light experiment for the Pt/n^+-GaN nanowires/n^+–p Si photocathode is 410,400 C cm^{-2} considering an average saturation photocurrent density of ~38 mA cm^{-2} for 3000 h. The presented platinized n^+-GaN nanowires/n^+–p Si photocathode for 3000 h operation had the same amount of charge passed during >1.5 years of outdoor operation under AM 1.5G one-sun conditions with a solar capacity of 20%.[5] As the projected operation is a lower limit on the actual stability of Pt/n^+-GaN nanowires/n^+–p Si, it is necessary to perform accelerated long-term stability tests with temperature and light intensity variations to precisely identify the degradation/corrosion mechanisms. Furthermore, Fig. 5(c) shows the amount of H_2 production (in Lit per cm^{-2}) under standard temperature and pressure (STP) conditions for some of the best reported long-term stable photocathodes[10,11,23,42,53] over the entire duration of the stability experiments. Compared to these photocathodes, the platinized n^+-GaN nanowires/n^+–p Si photocathode has the highest H_2 production of >45 Lit per cm^{-2}. These results, combined with the fact that GaN and Si are industry established materials, suggest the scalability and economic viability of this photocathode system for large-scale implementation of PEC water splitting. Recent studies show that the PEC characteristics for the n^+-GaN nanowires/n^+–p Si photocathode are further improved by using controllable Pt loading amounts through PEC photo-deposition.[51] In future studies, we will focus on *in situ* catalyst regeneration and identify approaches to eliminate Pt loading during PEC reaction, which can further reduce the H_2 production cost, to achieve ultrahigh stability and high efficiency.

We have also performed atomic force microscope (AFM) measurements of the GaN-protected Si photocathodes before and after chronoamperometry testing to compare the morphology changes due to photoelectrochemistry. Since such AFM measurements can only be performed on planar surfaces, nearly coalesced GaN nanostructures with a quasi-planar

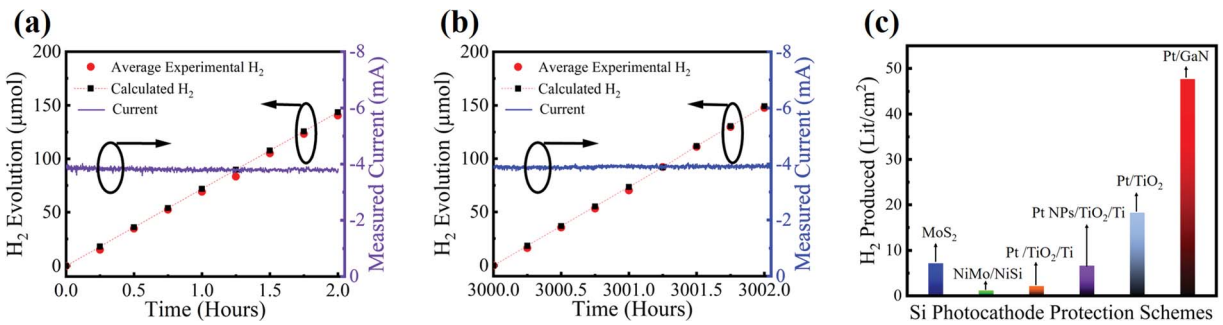

Fig. 5 Faraday efficiency of platinized n^+-GaN nanowires/n^+–p Si. H_2 generation for the platinized n^+-GaN nanowires/n^+–p Si photocathode at 0 V *vs.* RHE under AM 1.5G one-sun illumination in 0.5 M H_2SO_4 for (a) 0–2 h and (b) 3000–3002 h. The red dots represent the average amount of H_2 generated at various times, and the black dotted line is the theoretical amount of H_2 produced *vs.* time based on the photocurrent. The sample area is 0.12 cm^2 which corresponds to a photocurrent density of ~38 mA cm^{-2}. (c) Total H_2 production in Lit cm^{-2} at STP for Si based photocathodes with various protection schemes: MoS_2,[11] NiMo/NiSi,[53] Pt/TiO_2/Ti,[42] Pt NPs/TiO_2/Ti[10] and Pt/TiO_2.[23]

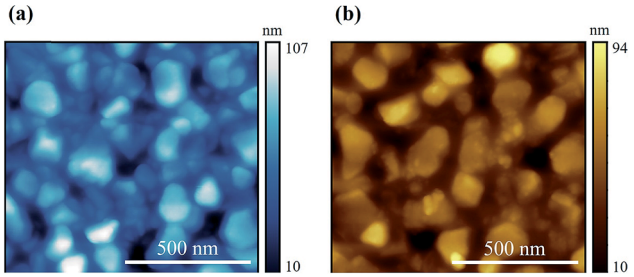

Fig. 6 AFM analysis of planar n^+-GaN on n^+–p Si. The pristine sample without Pt nanoparticles (a) before the reaction and (b) after the 10 h stability test in 0.5 M H_2SO_4 under AM 1.5G one-sun illumination.

morphology were used in this experiment. The measurement details are described in the Experimental section, ESI.† As shown in Fig. 6(a) and (b), no change in the surface morphology was observed for 10 h of the reaction, further confirming that GaN is intrinsically stable under harsh photocatalysis conditions. Studies were also performed by varying the thickness of the GaN surface protective layer (see Fig. S2, ESI†). The measured photocurrent densities (shown in Fig. S2, ESI†) are nearly the same for the samples studied, which is consistent with the near-perfect conduction band alignment between GaN and Si measured previously.[9]

The underlying mechanism for the unprecedentedly ultra-high stability of the GaN protected Si photocathode is described. Firstly, wurtzite GaN nanowires grown on a Si wafer are nearly free of dislocations due to the efficient surface strain relaxation and have strong ionic bonds which lead to bunching of surface states near the band edges.[48,54] Our previous studies suggest that the presented GaN nanostructures have unique N-termination, not only on the top *c*-plane surface but also on the lateral nonpolar surfaces, which can protect against photo-corrosion and oxidation.[48,50] As shown previously, there is also a thin GaN layer beneath the nanowires which protects the Si from the formation of insulating oxides and passivates the surface states to prevent charge carrier recombination.[9] Moreover, due to the negligibly small conduction band offset between Si and GaN there is virtually no loss in charge carrier extraction.[9] As such, the unique GaN nanostructures can protect the underlying Si surface against photo-corrosion with enhanced charge carrier extraction kinetics and better light absorption. The Pt/GaN interface further improves the charge carrier extraction compared to that of Pt/Si[9,51] and thereby enhances the overall stability of the photocathode. In future devices, the catalyst regeneration process can be minimized or eliminated by utilizing a more robust co-catalyst integration process, such as atomic layer integration.

Conclusion

In conclusion, we have demonstrated that the Pt/n^+-GaN nanowires/n^+–p Si photocathode can exhibit both high efficiency and long-term stable operation in three-electrode configuration. The unique GaN nanostructures can significantly enhance the performance of Si photocathodes (achieving a high photocurrent density of $\sim$38 mA cm^{-2} and an ABPE $\sim$ 11.9%) and further provide extremely robust protection for the Si surface for over 3000 h (>500 days) without any performance degradation, *i.e.*, without any loss of photocurrent, onset potential, or efficiency. Future work will include a more fundamental understanding of the surface properties of such GaN nanostructures and the underlying mechanism for the extraordinary stability in harsh PEC water splitting, and to perform long-term stability studies in two-electrode configuration. This unique PEC platform, by utilizing the two most produced semiconductors, *i.e.*, Si and GaN, lays a solid foundation for realizing practical PEC water splitting devices and systems that are efficient, stable, and low cost.

Acknowledgements

The authors gratefully acknowledge research support from the HydroGEN Advanced Water Splitting Materials Consortium, established as part of the Energy Materials Network under the U. S. Department of Energy, Office of Energy Efficiency and Renewable Energy, Fuel Cell Technologies Office, under Contract Number DE-EE0008086 for the University of Michigan, under Contract Number DE-AC52-07NA27344 for Lawrence Livermore National Laboratory, and under Contract Number DE-AC02-05CH11231 for Lawrence Berkeley National Laboratory. The authors acknowledge the support from National Science Foundation under grant CBET 1804458 and Emissions Reduction Alberta. The authors also acknowledge the financial support of the University of Michigan College of Engineering and NSF grant #DMR-0723032 and technical support from the Michigan Center for Materials Characterization.

References

1 Y. He, T. Hamann and D. Wang, *Chem. Soc. Rev.*, 2019, **48**, 2182–2215.
2 N. S. Lewis, *Science*, 2016, **351**, aad1920.
3 T. Lopes, P. Dias, L. Andrade and A. Mendes, *Sol. Energy Mater. Sol. Cells*, 2014, **128**, 399–410.
4 M. Dumortier, S. Tembhurne and S. Haussener, *Energy Environ. Sci.*, 2015, **8**, 3614–3628.
5 M. R. Shaner, H. A. Atwater, N. S. Lewis and E. W. McFarland, *Energy Environ. Sci.*, 2016, **9**, 2354–2371.
6 R. Fan, Z. Mi and M. Shen, *Opt. Express*, 2019, **27**, A51.
7 B. A. Pinaud, J. D. Benck, L. C. Seitz, A. J. Forman, Z. Chen, T. G. Deutsch, B. D. James, K. N. Baum, G. N. Baum, S. Ardo, H. Wang, E. Miller and T. F. Jaramillo, *Energy Environ. Sci.*, 2013, **6**, 1983.
8 S. Chu, W. Li, Y. Yan, T. Hamann, I. Shih, D. Wang and Z. Mi, *Nano Futures*, 2017, **1**, 022001.
9 S. Vanka, E. Arca, S. Cheng, K. Sun, G. A. Botton, G. Teeter and Z. Mi, *Nano Lett.*, 2018, **18**, 6530–6537.

10 B. Seger, D. S. Tilley, T. Pedersen, P. C. K. Vesborg, O. Hansen, M. Grätzel and I. Chorkendorff, *RSC Adv.*, 2013, **3**, 25902.

11 L. A. King, T. R. Hellstern, J. Park, R. Sinclair and T. F. Jaramillo, *ACS Appl. Mater. Interfaces*, 2017, **9**, 36792–36798.

12 J. D. Benck, S. C. Lee, K. D. Fong, J. Kibsgaard, R. Sinclair and T. F. Jaramillo, *Adv. Energy Mater.*, 2014, **4**, 1400739.

13 H. P. Wang, K. Sun, S. Y. Noh, A. Kargar, M. L. Tsai, M. Y. Huang, D. L. Wang and J. H. He, *Nano Lett.*, 2015, **15**, 2817–2824.

14 D. Kang, J. L. Young, H. Lim, W. E. Klein, H. Chen, Y. Xi, B. Gai, T. G. Deutsch and J. Yoon, *Nat. Energy*, 2017, **2**, 17043.

15 Q. Li, M. Zheng, M. Zhong, L. Ma, F. Wang, L. Ma and W. Shen, *Sci. Rep.*, 2016, **6**, 29738.

16 R. J. Britto, J. D. Benck, J. L. Young, C. Hahn, T. G. Deutsch and T. F. Jaramillo, *J. Phys. Chem. Lett.*, 2016, **7**, 2044–2049.

17 M. H. Lee, K. Takei, J. Zhang, R. Kapadia, M. Zheng, Y. Z. Chen, J. Nah, T. S. Matthews, Y. L. Chueh, J. W. Ager and A. Javey, *Angew. Chem., Int. Ed. Engl.*, 2012, **51**, 10760–10764.

18 J. Gu, Y. Yan, J. L. Young, K. X. Steirer, N. R. Neale and J. A. Turner, *Nat. Mater.*, 2016, **15**, 456–460.

19 F. Nandjou and S. Haussener, *J. Phys. D: Appl. Phys.*, 2017, **50**, 124002.

20 H. Kaneko, T. Minegishi and K. Domen, *Chem.–Eur. J.*, 2018, **24**, 5697–5706.

21 L.-J. Guo, J.-W. Luo, T. He, S.-H. Wei and S.-S. Li, *Phys. Rev. Appl.*, 2018, **10**, 064059.

22 K. W. Frese, M. J. Madou and S. R. Morrison, *J. Phys. Chem.*, 1980, **84**, 3172–3178.

23 D. Bae, B. Seger, O. Hansen, P. C. K. Vesborg and I. Chorkendorff, *ChemElectroChem*, 2019, **6**, 106–109.

24 D. Bae, B. Seger, P. C. Vesborg, O. Hansen and I. Chorkendorff, *Chem. Soc. Rev.*, 2017, **46**, 1933–1954.

25 H. Gerischer, *J. Electroanal. Chem. Interfacial Electrochem.*, 1975, **58**, 263–274.

26 S. Chen and L.-W. Wang, *Chem. Mater.*, 2012, **24**, 3659–3666.

27 S. Hu, M. R. Shaner, J. A. Beardslee, M. Lichterman, B. S. Brunschwig and N. S. Lewis, *Science*, 2014, **344**, 1005–1009.

28 S. W. Boettcher, E. L. Warren, M. C. Putnam, E. A. Santori, D. Turner-Evans, M. D. Kelzenberg, M. G. Walter, J. R. McKone, B. S. Brunschwig, H. A. Atwater and N. S. Lewis, *J. Am. Chem. Soc.*, 2011, **133**, 1216–1219.

29 H. J. Lewerenz, *J. Electrochem. Soc.*, 2014, **161**, H3117–H3129.

30 Y. Kuang, Q. Jia, G. Ma, T. Hisatomi, T. Minegishi, H. Nishiyama, M. Nakabayashi, N. Shibata, T. Yamada, A. Kudo and K. Domen, *Nat. Energy*, 2016, **2**, 16191.

31 P. Dias, A. Vilanova, T. Lopes, L. Andrade and A. Mendes, *Nano Energy*, 2016, **23**, 70–79.

32 N. P. Dasgupta, C. Liu, S. Andrews, F. B. Prinz and P. Yang, *J. Am. Chem. Soc.*, 2013, **135**, 12932–12935.

33 B. Fabre, G. Li, F. Gouttefangeas, L. Joanny and G. Loget, *Langmuir*, 2016, **32**, 11728–11735.

34 E. Kemppainen, A. Bodin, B. Sebok, T. Pedersen, B. Seger, B. Mei, D. Bae, P. C. K. Vesborg, J. Halme, O. Hansen, P. D. Lund and I. Chorkendorff, *Energy Environ. Sci.*, 2015, **8**, 2991–2999.

35 C. U. Maier, M. Specht and G. Bilger, *Int. J. Hydrogen Energy*, 1996, **21**, 859–864.

36 B. Zhou, X. Kong, S. Vanka, S. Chu, P. Ghamari, Y. Wang, N. Pant, I. Shih, H. Guo and Z. Mi, *Nat. Commun.*, 2018, **9**, 3856.

37 D. M. Andoshe, G. Jin, C.-S. Lee, C. Kim, K. C. Kwon, S. Choi, W. Sohn, C. W. Moon, S. H. Lee, J. M. Suh, S. Kang, J. Park, H. Heo, J. K. Kim, S. Han, M.-H. Jo and H. W. Jang, *Adv. Sustainable Syst.*, 2018, **2**, 1700142.

38 R. Fan, S. Cheng, G. Huang, Y. Wang, Y. Zhang, S. Vanka, G. A. Botton, Z. Mi and M. Shen, *J. Mater. Chem. A*, 2019, **7**, 2200–2209.

39 E. L. Warren, J. R. McKone, H. A. Atwater, H. B. Gray and N. S. Lewis, *Energy Environ. Sci.*, 2012, **5**, 9653.

40 M. T. McDowell, M. F. Lichterman, A. I. Carim, R. Liu, S. Hu, B. S. Brunschwig and N. S. Lewis, *ACS Appl. Mater. Interfaces*, 2015, **7**, 15189–15199.

41 R. Fan, W. Dong, L. Fang, F. Zheng and M. Shen, *J. Mater. Chem. A*, 2017, **5**, 18744–18751.

42 C. Ros, T. Andreu, M. D. Hernandez-Alonso, G. Penelas-Perez, J. Arbiol and J. R. Morante, *ACS Appl. Mater. Interfaces*, 2017, **9**(21), 17932–17941.

43 R. Fan, W. Dong, L. Fang, F. Zheng, X. Su, S. Zou, J. Huang, X. Wang and M. Shen, *Appl. Phys. Lett.*, 2015, **106**, 013902.

44 B. Mei, B. Seger, T. Pedersen, M. Malizia, O. Hansen, I. Chorkendorff and P. C. K. Vesborg, *J. Phys. Chem. Lett.*, 2014, **5**, 1948–1952.

45 X. H. Zhou, R. Liu, K. Sun, D. Friedrich, M. T. McDowell, F. Yang, S. T. Omelchenko, F. H. Saadi, A. C. Nielander, S. Yalamanchili, K. M. Papadantonakis, B. S. Brunschwig and N. S. Lewis, *Energy Environ. Sci.*, 2015, **8**, 2644–2649.

46 B. Seger, T. Pedersen, A. B. Laursen, P. C. Vesborg, O. Hansen and I. Chorkendorff, *J. Am. Chem. Soc.*, 2013, **135**, 1057–1064.

47 X. Chen and S. S. Mao, *Chem. Rev.*, 2007, **107**, 2891–2959.

48 M. G. Kibria, R. Qiao, W. Yang, I. Boukahil, X. Kong, F. A. Chowdhury, M. L. Trudeau, W. Ji, H. Guo, F. J. Himpsel, L. Vayssieres and Z. Mi, *Adv. Mater.*, 2016, **28**, 8388–8397.

49 X. Guan, F. A. Chowdhury, Y. Wang, N. Pant, S. Vanka, M. L. Trudeau, L. Guo, L. Vayssieres and Z. Mi, *ACS Energy Lett.*, 2018, **3**, 2230–2231.

50 J. Su, Y. Wei and L. Vayssieres, *J. Phys. Chem. Lett.*, 2017, **8**, 5228–5238.

51 Y. He, S. Vanka, T. Gao, D. He, J. Espano, Y. Zhao, Q. Dong, C. Lang, Y. Wang, T. W. Hamann, Z. Mi and D. Wang, *Nano Res.*, 2019, DOI: 10.1007/s12274-019-2346-3.

52 Z. Yin, R. Fan, G. Huang and M. Shen, *Chem. Commun.*, 2018, **54**, 543–546.

53 W. Vijselaar, R. M. Tiggelaar, H. Gardeniers and J. Huskens, *ACS Energy Lett.*, 2018, **3**, 1086–1092.

54 T. D. Moustakas, *Phys. Status Solidi A*, 2013, **210**, 169–174.